ELSEVIER

Contents lists available at ScienceDirect

International Journal of Solids and Structures

journal homepage: www.elsevier.com/locate/ijsolstr



Effects of buckling struts on the fracture toughness of triangular lattices

Melle Gruppelaar[®], Eral Bele[®], P.J. Tan[®]*

Department of Mechanical Engineering, University College London, Torrington Place, London WC1E 7JE, UK

ARTICLE INFO

Keywords:
Buckling
Fracture
Lattice materials
T-stress

ABSTRACT

The effect of strut-buckling on the fracture toughness of elastic-brittle triangular lattices is investigated using the finite element method. Buckling of struts in the vicinity of a crack-tip is shown to precede fracture contingent on the relative density and strut material. Under idealised *K*-field conditions, it was found that the buckling struts act as a toughening mechanism in Mode I loading and lead to a knockdown in fracture toughness in Mode II. Linear perturbation analyses reveal the transition relative density below which strut-buckling precedes fracture, and its dependence upon the fracture strain of the strut material. A power-law scaling relationship between fracture toughness and relative density is proposed for the regime where buckling of constituent struts can occur before fracture. It will be shown that strut-buckling can lead to elastic crack-tip blunting and to the development of compliant layers of cells with reduced stiffness. Subsequently, the effects of mode mixity and *T*-stress on the transition relative density and deviation from the traditional fracture toughness scaling law are addressed. Buckling struts act as a toughening mechanism in modes with predominantly Mode I influence and lead to a knockdown in toughness for modes with more than 25% Mode II contribution. The inclusion of negative *T*-stress leads to an increase in the transition relative density and to significant toughness knockdown after the onset of buckling in Mode I.

1. Introduction

Micro-architected lattices have attracted significant interest as lightweight and energy-efficient structural materials owing to their excellent mechanical properties. Of particular promise is their high weight-specific fracture toughness. Previous studies have shown that the fracture toughness (K_c) of a lattice obeys a power-law relationship of the form $K_c = D\overline{\rho}^d \sigma_0 \sqrt{l_0}$, where σ_0 is the failure strength of the cell wall material, l_0 is the characteristic cell size and $\bar{\rho}$ is the relative density (Schmidt and Fleck, 2001; Fleck and Qiu, 2006; Romijn and Fleck, 2007; Cui et al., 2011; Tankasala et al., 2015; Gu et al., 2018). In general, K_c depends on the microarchitecture of a lattice (whether it is stretch- or bending- dominated), its cell wall material properties, loading conditions (relative contributions of Mode I and/or Mode II loading), and higher-order deformation terms (such as T-stress). The aforementioned scaling law has been validated by experiments; see, for example, Huang and Gibson (1991), Quintana-Alonso et al. (2010) and Gu et al. (2018). However, others have reported divergences. For instance, Tankasala et al. (2015) showed that the fracture toughness of lattices are affected by finite strut(s) displacements.

Lattices can undergo elastic buckling under several loading conditions: in uniaxial compression (Chuang and Huang, 2002; Yang and Huang, 2005; Latture et al., 2018; He et al., 2018; Werner et al., 2022),

The focus of this paper is on triangular lattices, where the dominant deformation of its constituent struts is either axial stretch or compression. Depending on the relative density and whether the compressive force in a constituent strut is sufficiently high, elastic buckling can be triggered locally. The latter may cause geometric disruptions to its regular lattice frame-work, leading to changes in the local effective properties which, in turn, induces a change in the crack-tip asymptotic

E-mail address: pj.tan@ucl.ac.uk (P.J. Tan).

biaxial compression (Guo and Gibson, 1999; Okumura et al., 2004; Ohno et al., 2004), tensile loading (Fan et al., 2009; Tankasala et al., 2017), or shear (Haghpanah et al., 2014). Buckling has been observed locally, in single-cells or struts, and/or globally, affecting a large number of cells. Hitherto, there have been limited studies on the effects of geometric nonlinearities, *viz.* the elastic buckling of constituent struts, on the fracture toughness of lattice materials. In Quintana-Alonso and Fleck (2009), the possibility of strut-buckling was considered in compressively loaded diamond lattices containing a pre-crack. It was shown that strut buckling could occur before crack propagation due to the compressive components of the crack-tip field. The interactions between the finite deformations of buckled struts and the crack-tip displacement field are not yet well understood in lattices subjected to conventional Mode I or II loading, and the mechanisms that affect fracture in the post-buckling regime have not been investigated to date.

^{*} Corresponding author.

stress field. The consequence of this is deviations from the fracture toughness predicted by traditional scaling law.

This paper is organised as follows. First, the issue of whether constituent strut-buckling can occur in a triangular lattice before fracture is addressed and the range of relative densities over which this occurs is determined. Next, the influence of strut-buckling on the Mode I and II fracture toughness is quantified, and their effect on the crack opening displacement and local stiffness of the cells is addressed. Finally, the influence of mixed-mode loading and higher-order deformation terms (such as T-stress) on the fracture toughness are established.

2. Method

2.1. Background theory

The in-plane stress field around the crack-tip of an isotropic and homogenous linear-elastic body is given by (Williams, 1957)

$$\sigma_{ij} = A_1 \frac{g_{ij}^{(1)}(\theta)}{\sqrt{r}} + A_2 g_{ij}^{(2)}(\theta) + \sum_{n=2}^{\infty} A_n g_{ij}^{(n)}(\theta) r^{(n-2)/2}$$
 (1)

where σ_{ij} is the stress tensor; r and θ are the polar coordinates centered at the crack-tip; $g_{ij}^n(\theta)$ are dimensionless functions of θ ; and, A_n is the stress amplitude corresponding to the nth term. The first and second terms of Eq. (1) correspond to the K-field and T-stress, respectively.

In the immediate vicinity of the crack-tip, the singular stress field given by the leading term in Eq. (1) can be additively decomposed into contributions from the remote tensile (Mode I) and in-plane shear (Mode II) loadings as follows (Kanninen and Popelar, 1985)

$$\sigma_{ij} = \frac{K_{\mathrm{I}}}{\sqrt{2\pi r}} \hat{\sigma}_{ij}^{\mathrm{I}} + \frac{K_{\mathrm{II}}}{\sqrt{2\pi r}} \hat{\sigma}_{ij}^{\mathrm{II}} \tag{2}$$

where $K_{\rm I}$ and $K_{\rm II}$ are the Mode I and Mode II stress intensity factors (SIF), respectively. For mixed-mode loading, the relative composition of $K_{\rm I}$ and $K_{\rm II}$ is controlled by means of an elastic mode mixity parameter M given by (Sih, 1974)

$$M = \frac{2}{\pi} \tan^{-1} \left(\frac{K_{\text{II}}}{K_{\text{I}}} \right) \quad \text{and} \quad 0 \le M < 1$$
 (3)

where the limiting values of M=0 and $M\to 1^-$ correspond to the Mode I and Mode II fracture toughness, respectively.

The displacement (u_1, u_2) and rotation (ω) fields associated with the leading-order term in Eq. (1) in an elastic body in plane strain are (Kanninen and Popelar, 1985; Fleck and Oiu, 2006)

$$u_{1} = \frac{K_{\rm I}}{2G^{*}} \sqrt{\frac{r}{2\pi}} \cos \frac{\theta}{2} (\kappa - 1 + 2\sin^{2}\frac{\theta}{2}) + \frac{K_{\rm II}}{2G^{*}} \sqrt{\frac{r}{2\pi}} \sin \frac{\theta}{2} (\kappa + 1 + 2\cos^{2}\frac{\theta}{2}) \quad ,$$
(42)

$$u_{2} = \frac{K_{I}}{2G^{*}} \sqrt{\frac{r}{2\pi}} \sin \frac{\theta}{2} (\kappa + 1 - 2\cos^{2}\frac{\theta}{2}) - \frac{K_{II}}{2G^{*}} \sqrt{\frac{r}{2\pi}} \cos \frac{\theta}{2} (\kappa - 1 - 2\sin^{2}\frac{\theta}{2}) \quad \text{and}$$
(4b)

$$\omega = -\frac{1+\kappa}{4G^*} \left(\frac{K_{\rm I}}{\sqrt{2\pi r}} \sin\frac{\theta}{2} + \frac{K_{\rm II}}{\sqrt{2\pi r}} \cos\frac{\theta}{2} \right) \tag{4c}$$

where G^* and v_{ps}^* are the effective shear modulus and plane-strain Poisson's ratio of the lattice, and $\kappa = (3 - v_{ps}^*)/(1 + v_{ps}^*)$. Eq. (4) is easily modified to include the contributions of T-stress by adding the following additional terms to the respective displacement field (Christodoulou and Tan, 2013):

$$u_1 = \frac{(1 - v_{ps}^*)}{2G^*} Tr \cos \theta$$
 and (5a)

$$u_2 = -\frac{v_{\rm ps}^*}{2G^*} T r \sin \theta \ . \tag{5b}$$

The magnitude of the *T*-stress is typically expressed as a stress biaxiality ratio given by (Leevers and Radon, 1982)

$$B = \frac{T\sqrt{\pi a}}{K_{\text{off}}} \tag{6}$$

where a is the crack length. $K_{\rm eff}$ is the effective Stress Intensity Factor (SIF) as follows

$$K_{\text{eff}} = \sqrt{K_{\text{I}}^2 + K_{\text{II}}^2} \ . \tag{7}$$

2.2. Boundary-layer method and finite element model

The Boundary-Layer Method (or BLM for brevity), used previously by Schmidt and Fleck (2001), is employed here to determine the fracture toughness of planar triangular lattices. It involves imposing the displacement and rotation fields in Eqs. (4) and (5), to the boundary of a Representative Volume Element (RVE), shown schematically in Fig. 1a, with the crack-tip located at the geometric centre of the RVE. The applied fields are increased incrementally (through increasing $K_{\rm I}$ and/or T in Eqs. (4) and (5)), and the fracture toughness of the lattice corresponds to the applied fields when any of the constituent struts reach their fracture strain ε_0 . The choice of the first strut failure criterion to define fracture toughness is consistent with the methodology employed in previous studies in literature (Fleck and Oiu, 2006; Romijn and Fleck, 2007; Gu et al., 2019a; Christodoulou and Tan, 2013), and is grounded on the observation of typically unstable crack propagation that follows the initial strut failure in brittle lattices (Tankasala and Fleck, 2020; Hsieh et al., 2020).

The Finite Element Analysis (using ABAQUS/Standard) is performed to solve the aforementioned boundary value problem. Large displacement formulations are used throughout and the post-buckling analyses are conducted without relying on initial deformations to trigger buckling. Timoshenko beam elements (B22) with 5 section points were used to mesh the constituent struts, and convergence studies showed that at least 8 elements/strut are needed to accurately capture the geometric nonlinearity associated with strut buckling. A simplified Local Tensile Strain (LTS) criterion, identical to the one employed by Tankasala et al. (2015), is adopted here. Note that the BLM requires a sufficiently large RVE size to avoid interference between the crack-tip field and the displacement and rotation boundary conditions, and there must be no interactions between the buckled cells and the boundary of the RVE. A size convergence study is employed to satisfy the criteria above. The RVE is considered sufficiently large when the normalised fracture toughness, $K_{\rm Ic}/(\bar{\rho}\sigma_0\sqrt{l_0})$, varies less than 1% between consecutive size increments. Fig. 1(b) shows the typical RVE size convergence for a lattice of relative density $\bar{\rho} = 0.1$ loaded in Mode I. In this paper, RVE sizes ranging from 100×100 cells for $\bar{\rho} = 0.3$ to 1800×1800 cells for $\overline{\rho} = 0.02$ were used.

A linear perturbation analysis (LPA) is used to obtain initial estimates of transition relative densities. The method involves solving an eigenvalue problem representing the buckling load factors. The Linear Perturbation Analysis (LPA) gives the eigenvalue, λ , associated with the first (fundamental) mode, representing the minimum multiplier of the imposed SIF, K, in Eq. (4), needed to activate strut buckling. As such, the SIF that activates buckling, K_{λ} is given by $K_{\lambda} = \lambda K$. The geometry and boundary conditions used in the LPA are identical to those of the conventional BLM, with the displacement field of the Williams expansion imposed on the edges of a Representative Volume Element.

The in-plane elastic modulus of the triangular lattice is $E^* = \frac{1}{3}\overline{\rho}E_s$, and in the out-of-plane direction the elastic modulus is $E^*_{33} = \overline{\rho}E_s$, while the Poisson's ratio is $v^*_{31} = v^*_{32} = v_s$ (Gibson and Ashby, 1997). Note that the elastic properties of the lattice were obtained under planestress conditions and they must be modified to give their plane-strain equivalents before they can be used in Eq. (4). Under plane-strain conditions, where $E^*_{33} = 0$ and $D^*_{33} = v^*_{31}D^*_{11} + v^*_{32}D^*_{22} = v_s(\sigma^*_{11} + \sigma^*_{22})$,

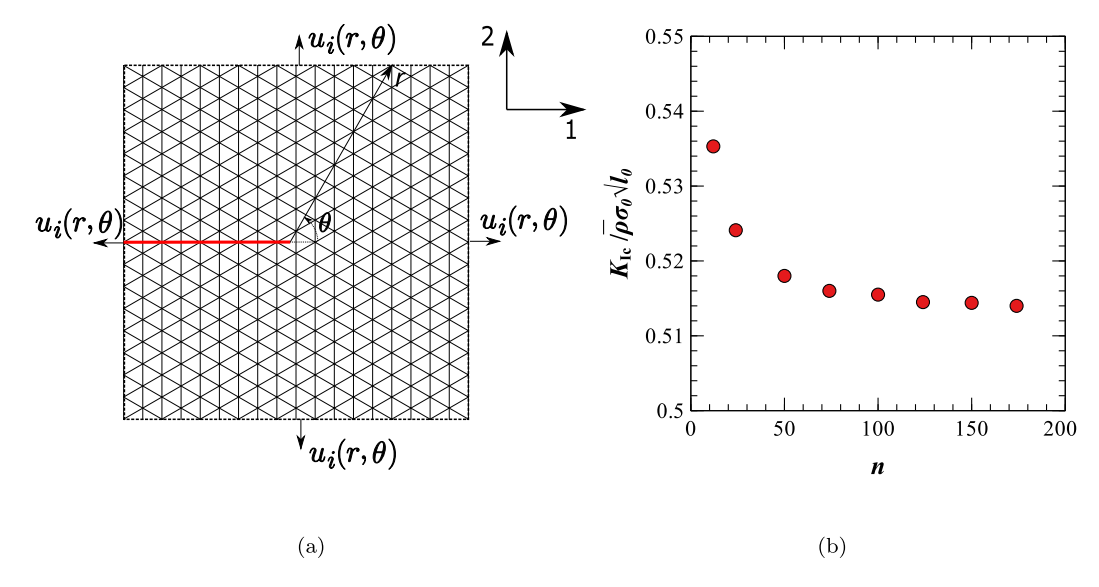


Fig. 1. The Boundary-Layer Method (BLM): (a) joint displacements $u_i(r,\theta)$ (i=1 or 2) and rotation ω , given in Eq. (4), prescribed around the boundary of a RVE; and, (b) variation of the normalised Mode I fracture toughness versus size of RVE for $\overline{\rho} = 0.1$. Solid red line indicates the pre-crack.

the modified elastic moduli and Poisson's ratio become (Romijn and Fleck, 2007)

$$E_{\rm ps}^* = \frac{3E^*}{3 - v_{\rm s}^2}$$
 , $v_{\rm ps}^* = \frac{1 + v_{\rm s}^2}{3 - v_{\rm s}^2}$ and $G^* = \frac{E_{\rm ps}^*}{2(1 + v_{\rm ps}^*)}$ (8)

3. Strut buckling under Mode I and II loading

The fracture toughness of a triangular lattice scales with relative density according to a power-law relationship given by (Fleck and Qiu, 2006)

$$K_c/\sqrt{l_0}\sigma_0 = D\overline{\rho}^d \tag{9}$$

where d=1 and D=0.50 in Mode I and D=0.38 in Mode II, for a triangular lattices, and the terms σ_0 and ε_0 refer to the failure stress and strain of the cell wall material, respectively. It must be emphasised that Eq. (9) does not take geometric nonlinearity into account. In this section, the possibility of strut buckling before fracture will be considered and its effects on the fracture toughness of a triangular lattice is quantified.

3.1. Linear perturbation analysis

A LPA is first performed to quantify the SIF that activates strut buckling. The purpose is to compare the K_{λ} results to the theoretical fracture toughness of the lattice and establish a critical relative density below which buckling can precede fracture. Eigenvalues are estimated for triangular lattices with relative density in the range $0.05 < \overline{\rho} < 0.2$ and the value of K_{λ} was fit against l_0 , E_S and $\overline{\rho}$, as follows:

$$K_{\mathrm{L}\lambda} = 0.794 \sqrt{l_0} E_S \bar{\rho}^3 \quad \text{and} \tag{10a}$$

$$K_{\text{II}\lambda} = 0.075 \sqrt{l_0} E_S \overline{\rho}^3$$
 (10b)

Fig. 2 shows the scaling of the normalised fracture toughness, $K_{\rm c}/\sqrt{l_0}\sigma_0$, and the SIF that activates buckling, expressed as $K_{\lambda}/\sqrt{l_0}E_S\varepsilon_0$, for three choices of ε_0 . Buckling may be activated when K_{λ} is smaller than the theoretical $K_{\rm Ic}$ or $K_{\rm IIc}$. The transition relative density, $\overline{\rho}_T$, corresponds to the intersection of the fracture toughness and buckling initiation curves. A general expression of the transition relative density, for any ε_0 , can be obtained by equating $K_{\rm c}$ and K_{λ} , resulting in an expression of the form

$$\overline{\rho}_T = Q\sqrt{\varepsilon_0} \tag{11}$$

where Q = 0.79 in Mode I and Q = 2.24 in Mode II. This expression encapsulates all the geometric and material parameters that affect buckling initiation in brittle linear elastic struts, and can be used to estimate the range of relative densities where buckling can occur before tensile fracture in Mode I and Mode II. For 18Ni-300 Steel, with its typical fracture strain of $\varepsilon_0 = 0.012$ (Kempen et al., 2011), a transition relative density of $\bar{\rho}_T = 0.08$ and $\bar{\rho}_T = 0.2$ may be expected in Mode I and II, indicating that strut buckling may precede fracture for relative densities that are encountered in practice. The normalised fracture toughness follows a linear scaling, while the buckling initiation curve is proportional to the cube of the relative density. The transition relative density follows the square root of the failure strain of the base material. Similar scaling relationships for buckling initiation and transition relative density have been observed for triangular and Kagome lattices without a crack in Mane et al. (2024). Exploring the impact of strut buckling on the fracture toughness of other stretch-dominated lattices may be of interest for future research.

The fracture toughness results in Sections 3.2, 3.3, 3.4 and 4 refer to a material with $\varepsilon_0=0.01$. Examples of other materials are provided in Section 4.1.

3.2. Effects of buckling struts on K_{Ic} and K_{IIc}

Fig. 3 shows the deformed mesh at the instant of failure in lattices with relative densities below and above the transition relative density in Mode I (a, b) and Mode II (c, d). The first struts to buckle and fracture are marked *B* and *F*, respectively. At low relative densities, several struts can buckle before fracture, forming a compliant layer of cells propagating perpendicularly to the pre-crack in Mode I and at a 30-degree angle in Mode II. Fracture occurs ahead of the crack-tip for lattices with relative density above the transition relative density. Below the transition relative density, the fracture location remains at the same strut in Mode I, but shifts to the location of the first buckled strut in Mode II.

An insight into the sequence of deformation mechanisms that lead to fracture can be obtained by examining the strain evolution in struts with the maximum tensile and compressive stresses ('T' and 'C' respectively). Fig. 4 shows the axial strain, ε_x , evolution up to fracture ($\varepsilon_0=0.010$) at two opposing surfaces of the compressive strut (ABAQUS section points: SP1 and SP5), and at the tensile strut, plotted against the normalised axial force in the local coordinate system, F_x/F_{cr} , where

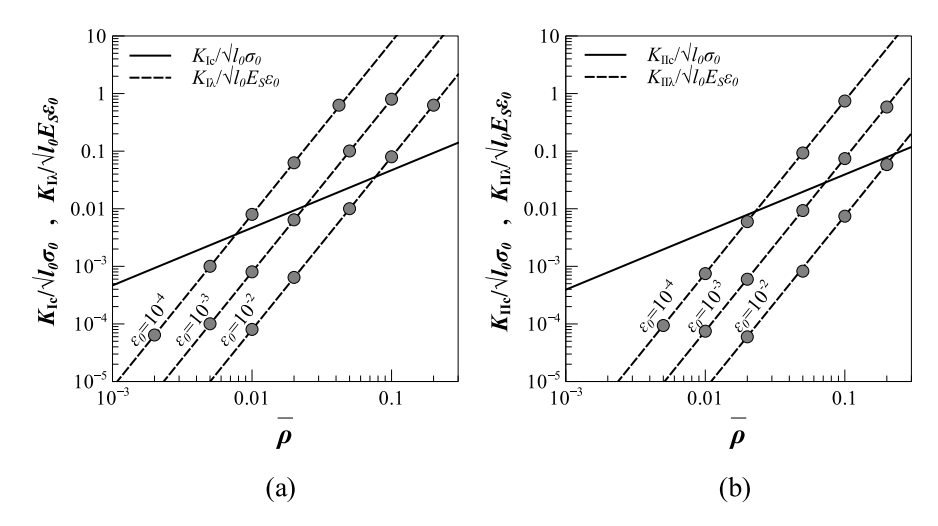


Fig. 2. Scaling of normalised fracture toughness, $K_c/\sqrt{l_0}\sigma_0$, and buckling initiation, $K_\lambda/\sqrt{l_0}E_S\varepsilon_0$, in Mode I (a) and Mode II (b) with the relative density, $\overline{\rho}$.

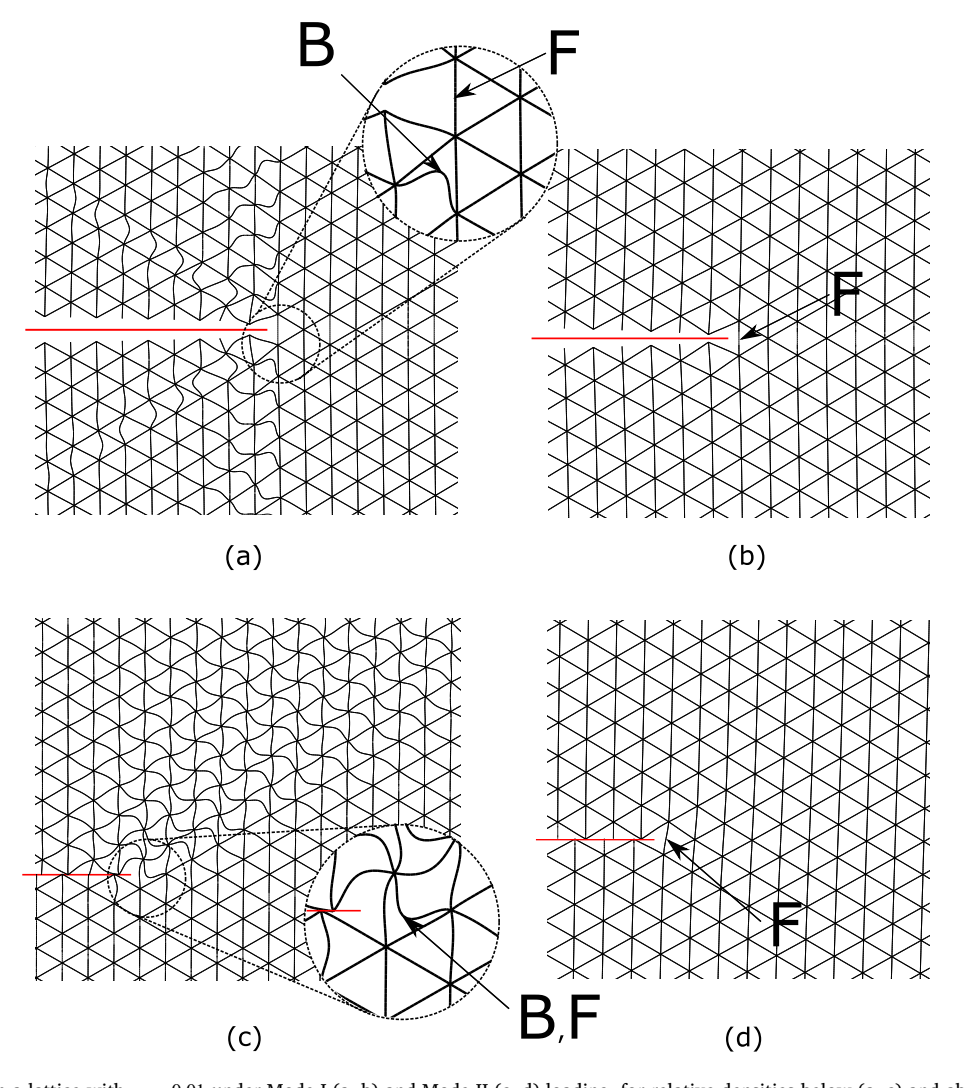


Fig. 3. Deformed mesh in a lattice with $\epsilon_0=0.01$ under Mode I (a, b) and Mode II (c, d) loading, for relative densities below (a, c) and above (b, d) the transition relative density. The relative densities are $\bar{\rho}=0.04$ (a), $\bar{\rho}=0.1$ (b), $\bar{\rho}=0.085$ (c) and $\bar{\rho}=0.25$ (d). Solid red lines indicate the pre-crack. Figures truncated to the vicinity of the crack-tip for the purpose of comparison.

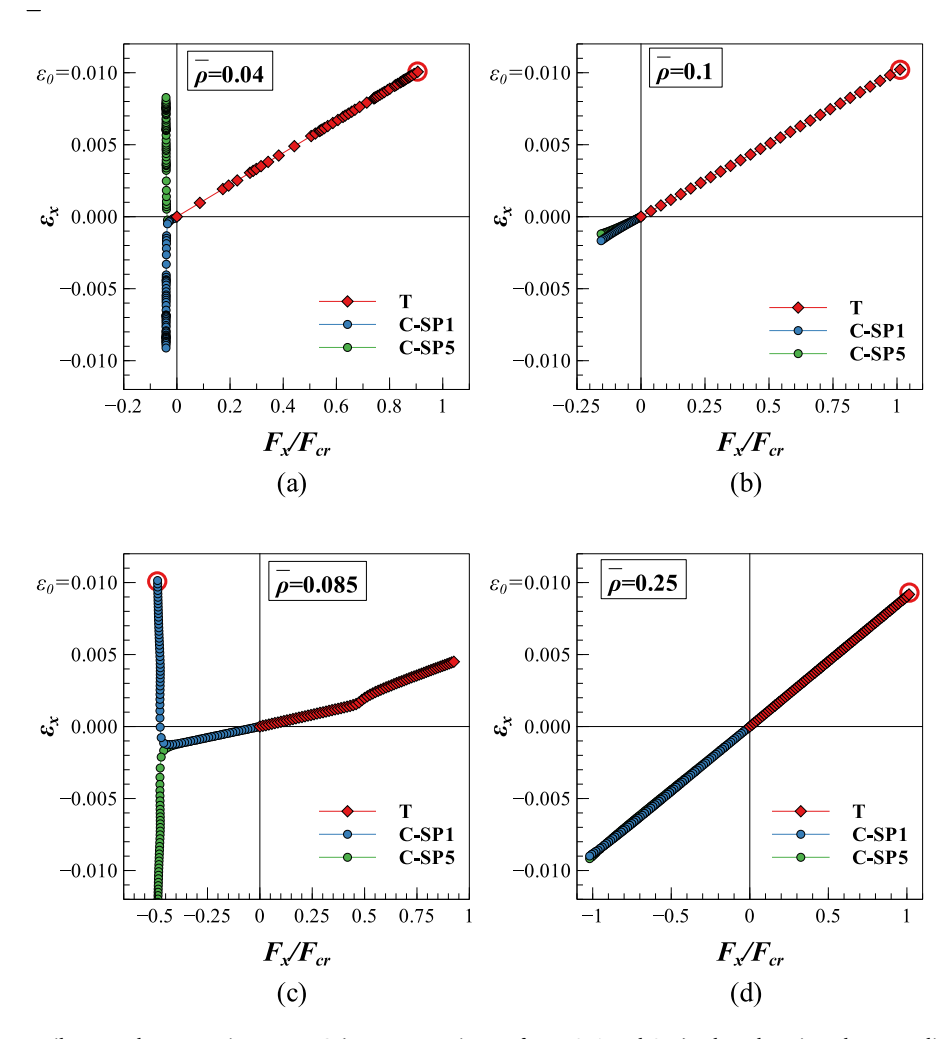


Fig. 4. Strain evolution in tensile, T, and compressive struts, C (at two opposing surfaces: SP1 and SP5), plotted against the normalised axial force in the local coordinate system, F_x/F_{cr} for relative densities below (a, c) and above (b, d) the buckling transition relative density, in Mode I (a, b) and Mode II (c, d).

 F_{cr} is the expected maximum tensile load at the instant of fracture, as derived from the fracture toughness scaling law, and given by

$$F_{cr} = \frac{K_{\rm c} A_S}{D \bar{\rho}^d \sqrt{I_0}} \tag{12}$$

where A_S is the cross-sectional area of the strut. In the absence of strut buckling (Fig. 4b and d), the strain evolution is linear in compressive and tensile struts. The tensile strain increases towards ε_0 , which is registered in the strut ahead of the crack-tip, as mentioned above. Conversely, at relative densities below the buckling transition relative densities (Fig. 4a and c), the strain evolution in the compressive struts indicates the typical post-buckling strain path bifurcation of columns in compression (Shanley, 1947): both edges initially develop negative strains, followed by strain bifurcation and reversal after the onset of buckling. In Mode II, after buckling, the strain path reaches the fracture strain in the buckled strut before achieving this condition in the tensile strut, and fracture occurs before the scaling law prediction. In Mode I, in spite of the existence of buckled struts, the tensile strut reaches the fracture strain first.

The effect of strut-buckling on the normalised $K_{\rm c}$ scaling is shown in Fig. 5. A transition distinguishes two fracture regimes: one where buckling does not occur before fracture and a second where strut buckling occurs before fracture, and the fracture toughness deviates from the original scaling law. Both regimes follow a power-law scaling of the form given in Eq. (9), with the pre-exponents D (above the buckling transition relative density) and $D^{(b)}$ (below the buckling transition relative density) shown in Table 1, and exponent d=1.

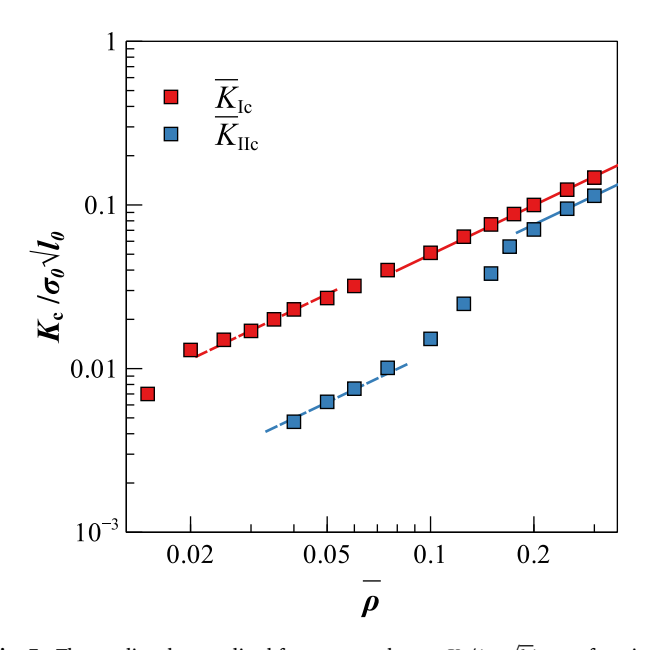


Fig. 5. The predicted normalised fracture toughness, $K_{\rm c}/(\sigma_0\sqrt{I_0})$, as a function of relative density, $\bar{\rho}$, under Mode I and II loading ($\epsilon_0=0.010$). Solid and dashed lines represent the power law fits to the normalised fracture toughness in the absence of buckling and after the onset of buckling, respectively.

Table 1 Values of fracture toughness scaling law pre-exponents, D and $D^{(b)}$, in the absence of strut-buckling and for fracture after the onset of strut-buckling, respectively, and transition relative density coefficients, Q, under different load mixities. M.

M	0	0.25	0.50	0.75	1
D	0.50	0.50	0.47	0.43	0.38
$D^{(b)}$	0.57	0.47	0.22	0.14	0.12
Q	0.79	0.98	1.52	1.95	2.24

The scaling relationship shows that the divergence from the established relationship is significant for Mode II loading. The deviation starts between 0.2 < $\bar{\rho}$ < 0.25 (note: LPA prediction $\bar{\rho}_{II_T}=0.212$), and settles to a new scaling relationship at $\bar{\rho}=0.075$. The knockdown factor in the pre-exponent of the scaling law is $D^{(b)}/D=0.32$. In Mode I the deviation starts between 0.06 < $\bar{\rho}$ < 0.075 (note: LPA prediction $\bar{\rho}_{I_T}=0.075$), and settles to a new scaling relationship when $\bar{\rho}$ < 0.05. In this loading mode, strut buckling provides a slight toughening mechanism, with $D^{(b)}/D=1.14$. At even lower relative densities ($\bar{\rho}$ < 0.02) the fracture toughness drops below the scaling law, and the fracture location switches to that of the buckled strut.

3.3. Influence of strut-buckling on crack opening displacement and local stiffness of the cells

Several mechanisms can affect the fracture toughness in solid materials with compliant zones, such as crack-deflection, crack-bridging, crack-branching, microcracking, plasticity induced crack-closure, and material heterogeneity (Hossain et al., 2014). In this paper, two features that may lead to the reported knockdown and increase in fracture toughness are addressed: crack-tip blunting in Mode I, and local knockdown in the modulus of the lattice.

Crack blunting is a well-known toughening mechanism in elastoplastic materials. The blunting magnitude and Crack Opening Displacement (COD) are associated to an increase in fracture toughness, as shown by Irwin (1957) and Dugdale–Barenblatt strip yield model (Dugdale, 1960; Barenblatt, 1962). In lattices, crack blunting can be activated in an elastic crack-tip stress field through bending layers in globally stretch-dominated geometries (Fleck and Qiu, 2006). A toughening effect has been reported in kagome lattices, where the reduced stiffness in the locally bending-dominated cells results in an elastic crack blunting phenomenon (Fleck and Qiu, 2006).

For the triangular lattices examined here, Fig. 6 shows the normalised COD at the instant of fracture $(\delta_y E_{ps}^*/K_{\rm Ic} \sqrt{l_0})$, where δ_y is the vertical displacement u_2 of nodes in the crack plane) against the normalised distance from the crack-tip along the crack-plane, x/l_0 . Three relative densities, in the presence $(\bar{\rho}=0.040,0.030)$ and absence $(\bar{\rho}=0.075)$ of strut buckling are considered. The analytical prediction obtained from the K-displacement field (Eq. (4b)) is shown for reference. At $\bar{\rho}=0.075$, the COD follows the theoretical prediction closely; however, at relative densities where strut-buckling precedes fracture $(\bar{\rho}=0.030)$ and $\bar{\rho}=0.040)$, the COD shapes indicate that elastic crack-blunting will occur and its magnitude increases with decreasing relative density. These results indicate that the development of compliant layers due to strut-buckling lead to crack-tip blunting and may be responsible for the slight toughening observed in Mode I loading.

Stretch-dominated lattices may be subject to bending boundary-layers that locally affect the stiffness of the lattice due to the reduced connectivity at free surfaces (Phani and Fleck, 2008). Next, the possibility of bending layers existing in the interior of the lattice in the post-buckled state and their effect on the stiffness of the constituent triangular cells are addressed.

Conventionally a unit-cell analysis is employed to obtain the elastic modulus of the lattice (e.g. Wang and McDowell, 2014). However, this analysis does not account for any edge effects or finite displacements of

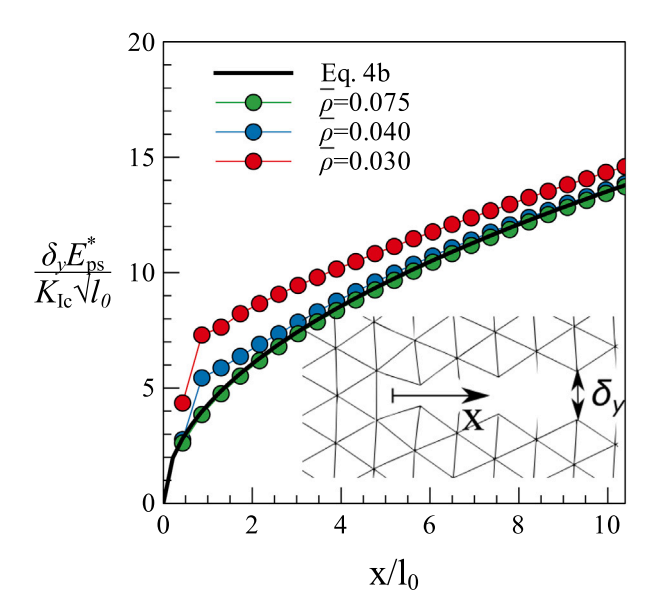


Fig. 6. Mode I normalised crack opening displacement, $\delta_{y}E_{ps}^{*}/K_{lc}\sqrt{l_{0}}$, at the instant of failure. Nodal coordinates along the *X*-axis normalised to the characteristic unit-cell length, l_{0} . The solid line represents the analytic prediction obtained from the *K*-field in Eq. (4b).

the struts. To illustrate the effect of buckling on the local elastic modulus, $E_{loc,x}^*$, the deformed lattice geometry at the instance of fracture is used. The FE mesh at that instant is divided into individual single-cell blocks and each cell is loaded in compression with boundary conditions that imply periodicity and hexagonal symmetry, as illustrated in Fig. 7. The local moduli are obtained through the following equation

$$E_{loc,x}^* = \frac{FL_x}{dL_y} \tag{13}$$

where F is the applied force per unit depth of the struts, L_x and L_y are the cell dimensions in the X and Y direction, and d is the resultant displacement.

Fig. 7 shows contour maps of the stiffness knockdown, $E_{loc.x}^{*}/E_{ps}^{*}$ at relative densities of 0.075, 0.05 and 0.04 in Mode I and 0.1, 0.075 and 0.05 in Mode II. A minimal knockdown in local stiffness is observed for lattices above the critical relative density. By contrast, zones with reduced stiffness are developed after the onset of buckling, at 90-degrees to the crack surface in Mode I and 30-degrees in Mode II. The magnitude of stiffness degradation and the number of affected cells increase with decreasing $\bar{\rho}$. At the lowest relative density, the stiffness degradation area extends to regions more than ten cells from the crack-tip and the stiffness reaches as low as 60% and 20% of the value of the undeformed lattice in Mode I and II, respectively. The reduction of effective stiffness due to buckling had also been observed in Mane et al. (2021).

The stiffness degradation area corresponds to the location of buckled cells in Fig. 3. In Mode II, the first strut failure location also occurs within the cells with reduced properties. In Tankasala and Fleck (2020), the Mode II crack-propagation follows a similar path (30-degree angle) to the buckling propagation and stiffness degradation zones shown here.

It should be noted that the non-homogeneous stiffness violates the BLM assumption of uniform material properties. However, the fracture toughness increase in Mode I agrees with the reported effect of heterogeneous material properties on the fracture toughness of solid materials with compliant layers. In these materials, the heterogeneous media increases the fracture toughness relative to the medium's bulk fracture toughness (Hossain et al., 2014), and the stress singularity near the crack-tip continues to be described by the singular term habitual

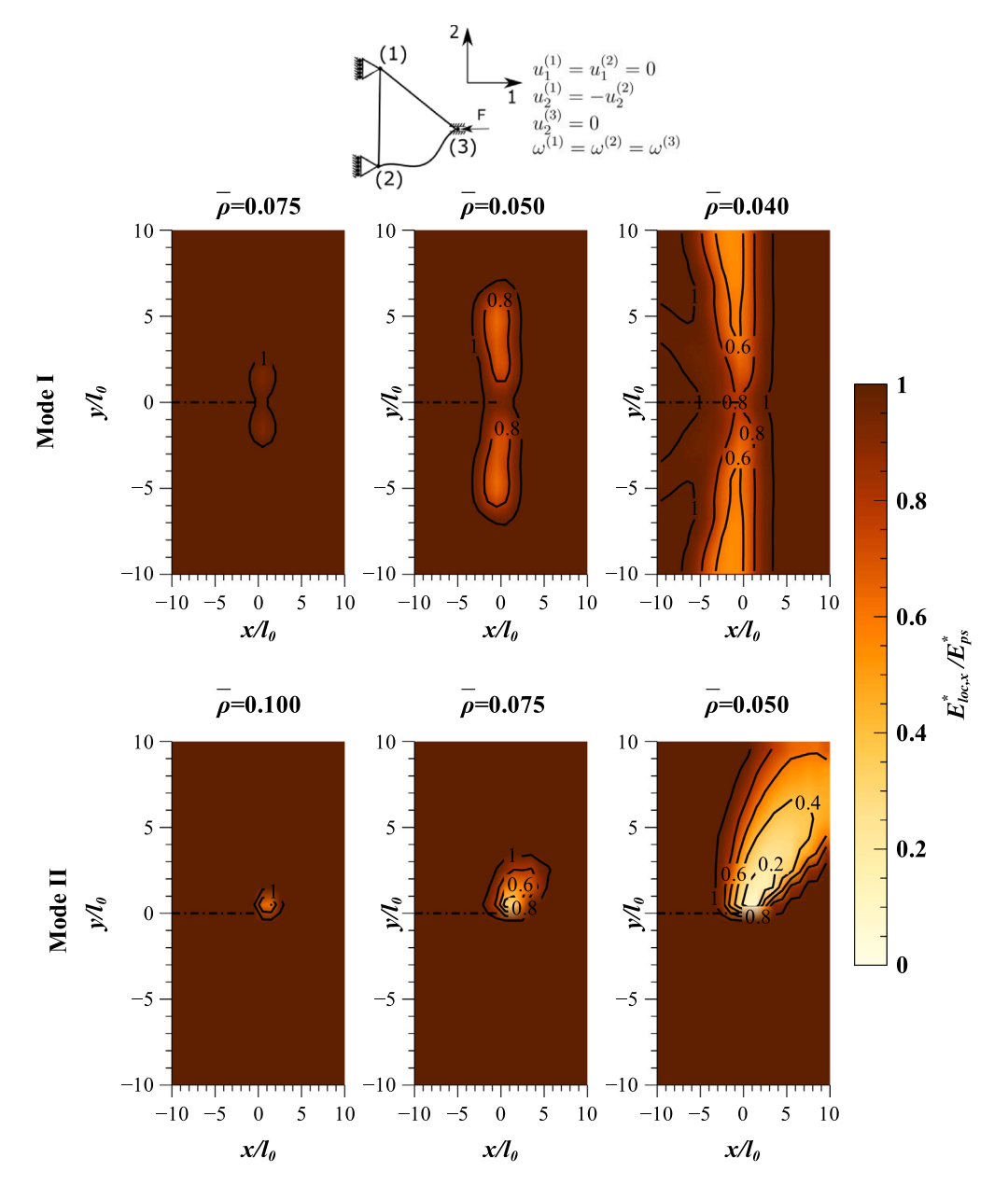


Fig. 7. Distribution of effective stiffness of the cells, $E_{ps.}^*/E_{ps.}^*$ in Mode I and Mode II, where x/I_0 and y/I_0 are the normalised coordinates relative to the crack-tip. Figures truncated to the vicinity of the crack-tip for the purpose of comparison.

of linear elastic fracture mechanics (Eischen, 1987). For heterogeneous materials the stress-field (Eq. (1)), is a function of the local variations in Modulus (Erdogan, 1995; Rousseau and Tippur, 2002). For this reason, a sufficiently sizeable RVE that entirely envelops the buckling-affected zone is necessary for the remote boundary condition presumed by the deformation state at the crack-tip to be valid. In some cases, the RVE size may become too large for practical computation; for example, to obtain the elimination of edge effects at $\bar{\rho}=0.02$ in Mode I a RVE of 1800×1800 cells is necessary. The full effect of buckling on fracture toughness and the effect of the finite-size needs to be validated using standardised experimental specimens, which is left to a later study.

An alternative method to the crack-tip field-based fracture toughness approach discussed in this study is the energy-based approach, as explored in the works of Luan et al. (2022) and Mane et al. (2024). Strut buckling can affect the estimated energy release, and future research should account for this by incorporating the distributed damage or non-local energy dissipation (Mane et al., 2024; Deng et al., 2023). The effects of strut buckling on the damage distribution can be summarised

as follows. Firstly, the field of buckled struts can extend to regions far from the crack tip, thus dissipating the elastic energy over a large area. This deformation mechanism, in turn, creates regions with a lower local effective stiffness, and leads to crack blunting, which effectively increases the total energy required for crack propagation. Secondly, strut buckling can cause sudden, non-recoverable energy dissipation through the abrupt failure of buckled struts, potentially reducing the predicted fracture toughness. In the presence of strut buckling, an energy-based approach should incorporate both of these possibilities.

3.4. Effects of crack orientation on the post-buckling fracture

The crack orientation and arrangement of the struts at the crack tip discussed thus far represent a crack traversing through nodes and vertical struts. However, the fracture toughness of the triangular lattice is anisotropic, depending on both the crack orientation relative to the lattice and the specific arrangement of the struts at the crack tip. The preceding and other possible configurations are presented in Fig.

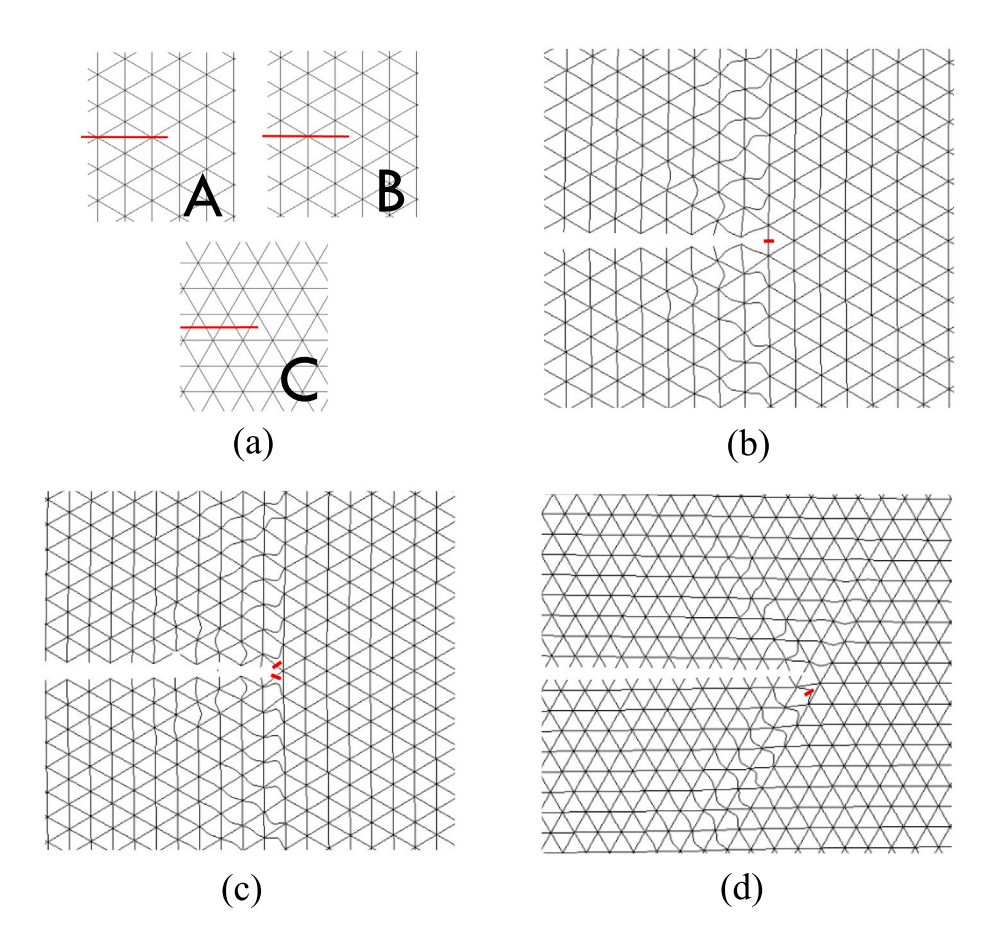


Fig. 8. Crack configurations for triangular lattices and deformation mesh in a lattice with $\bar{\rho} = 0.04$. Solid red lines indicate the pre-crack. Figures truncated to the vicinity of the crack-tip for the purpose of comparison.

Table 2 Fracture toughness scaling pre-exponent before, D, and after, $D^{(b)}$, buckling, obtained for crack configurations A, B and C.

Crack configuration	D (No buckling)	$D^{(b)}$ (Post-buckling)
A	0.50	0.53
В	0.56	0.59
C	0.64	0.63

8(a). The BLA was employed to determine the fracture toughness of crack configurations A, B and C across a range of relative density of $0.04 \le \overline{\rho} \le 0.3$. The deformation, strut buckling patterns, and fracture locations of a lattice with $\overline{\rho}=0.04$ are shown in Fig. 8 (b), (c) and (d). All three lattice configurations exhibit crack-tip blunting, and the deviation of their fracture toughness from the unbuckled scaling occurs at $\overline{\rho}\approx 0.075$. Their fracture toughness scales with exponent d=1 and their pre-exponents are presented in Table 2.

Configuration A exhibits the lowest fracture toughness across all relative densities. In contrast, configuration B results in an increase in fracture toughness of up to 12% relative to configuration A. The post-buckling fracture behaviour of lattices in configuration B follows a trend similar to that of configuration A, including similar buckling patterns perpendicular to the crack, crack-blunting, and an increase in the fracture toughness relative to the unbuckled state $(D^{(b)}/D=1.05)$. The higher fracture toughness in configuration B can be attributed to the presence of two oblique struts ahead of the crack tip.

The nucleation of cracks passing through oblique struts from an initial flaw, forming crack configuration C, has been observed in the works of Cherkaev and Ryvkin (2019), and may be more prevalent in practice. This configuration gives the highest fracture toughness at

the relevant range of relative density studied in this work, regardless of the occurrence of buckling. The increased fracture toughness aligns with findings from Lipperman et al. (2007) and Gu et al. (2018). The post-buckling behaviour in this configuration exhibits some differences relative to configurations A and B: the field of buckling struts is no longer predominantly perpendicular but favours a 60-degree angle backward from the crack plane, the fracture location occurs at buckled struts, and the post-buckling fracture toughness is slightly lower compared to the unbuckled scaling law $(D^{(b)}/D=0.98)$. In this crack orientation, the toughening effects of crack blunting are counteracted by increased compressive loading at the struts surrounding the crack tip, leading to the earlier strut fracture in a buckled strut.

Finally, it is important to note that this work analysed a linear crack path. However, other initial crack patterns are possible (e.g., as discussed in Cherkaev and Ryvkin, 2019) and could lead to distinct fracture behaviour if, for example, the pattern induces fracture in a buckled strut.

4. Effects of mixed-mode loading and T -stress

4.1. Effects of mode mixity

In this section, the effect of the relative contribution of Mode I and Mode II loading on $K_{\rm c}$ is addressed. Similarly to above, a LPA is first employed to obtain the transition relative densities, and the BLM to predict the fracture toughness knockdown in selected mode mixities. The mode mixity parameter M is used to quantify the relative composition of Modes I and II.

The transition relative density constants, Q, under different modemixity, are obtained and given in Table 1. Fig. 9(a) shows the critical

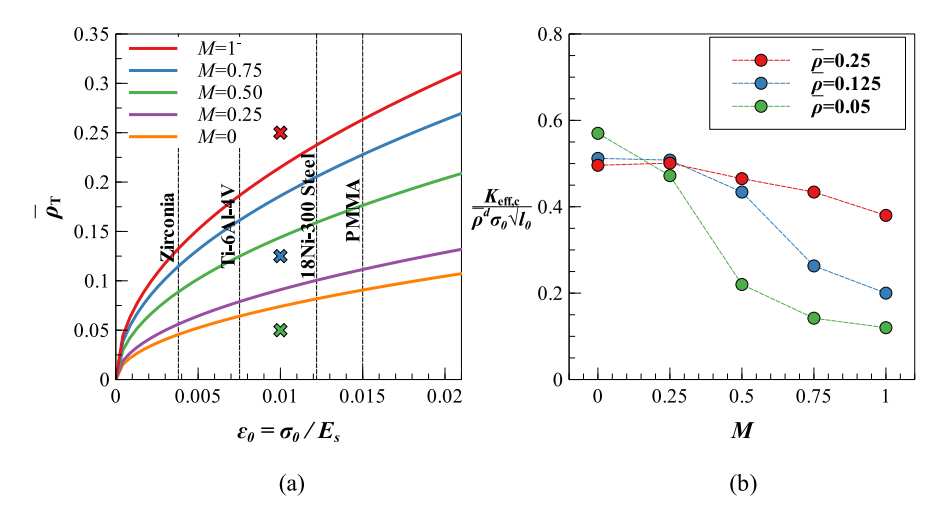


Fig. 9. Critical transition relative density, $\bar{\rho}_T$, as a function of material fracture strain, ϵ_0 , for five indicative mode mixities, M (a); and normalised fracture toughness as a function of mode mixity for a lattice with $\epsilon_0 = 0.01$ at three relative densities (shown as crosses in Figure (a)) (b).

transition relative densities from Eq. (11), as a function of the strain at failure, ε_0 . The relationships obtained under Mode I and II provide the boundaries of the transition relative density envelope, and lattices of materials with a higher ε_0 are likely to buckle before fracture at larger relative densities. For illustration purposes, four elastic-brittle materials are indicated: laser-cut PMMA, $\varepsilon_0=0.015\pm0.007$ (Seiler et al., 2019); 18Ni-300 steel (SLM produced), $\varepsilon_0=0.012\pm0.001$ (Kempen et al., 2011); Ti-6Al-4V, $\varepsilon_0=0.008\pm0.001$ (Li et al., 2008; Xiao et al., 2015) and Zirconia (partially stabilised), $\varepsilon_0=0.004$ (Noguchi et al., 1989).

The effect of buckling on $K_{\rm eff,c}$ (defined in Eq. (7)) is now analysed using the BLM. In Fig. 9(b) the effect of mixed-mode loading is examined in three relative density regimes of a lattice with $\varepsilon_0=0.01$ (marked with crosses in Fig. 9(a)): $\overline{\rho}=0.25$ (above the transition relative density in all modes), $\overline{\rho}=0.125$ (above the transition relative density in M=0,0.25), and $\overline{\rho}=0.050$ (below the transition relative density in all modes). Here, the fracture toughness is further normalised by $\overline{\rho}^d$, such that at $\overline{\rho}=0.25$ and $\overline{\rho}=0.050$, $K_{\rm eff,c}/(\overline{\rho}^d\,\sigma_0\sqrt{l_0})$ represents the pre-exponent D and $D^{(b)}$ of the scaling law.

The results indicate that in mode mixities where buckling does not precede fracture (e.g. M=0.0.25 for $\overline{\rho}=0.125$), the fracture toughness remains unchanged from the conventional scaling laws, as expected. In other mode mixities, where fracture occurs after strutbuckling, three regimes of influence are observed: (i) strut buckling induces a toughening mechanism when the initial strut fracture occurs at a tensile-loaded strut near the crack front (M<0.25), (ii) strut buckling has a minimal effect on fracture toughness (M=0.25), and (iii) a reduction of fracture toughness when the first strut to fracture is a buckled strut (M>0.25). In the latter regime, the fracture toughness knockdown becomes more severe at mode mixities that contain a larger proportion of Mode II loading.

4.2. Effects of T -stress

In experimental fracture toughness tests, T-stress and higher-order stress terms in the Williams expansion commonly present. Typical values of the T-stress term, quantified by the biaxiality ratio, B, in Eq. (6), are -0.5 < B < -0.1 for Single Edge Notched Tension specimens, -0.5 < B < 0.3 for Single Edge Notched Bending specimens, B = -0.5 for Double Edge Notched Tension specimens and B = -1 for Compact Tension specimens (Leevers and Radon, 1982; Anderson, 1995). In lattices where strut buckling is not present the T-stress term does not significantly affect the fracture toughness measurements (Gu et al., 2019a). However, its influence on $K_{\rm c}$ after the onset of strut-buckling is unknown.

Table 3 Value of buckling transition relative density coefficients in pure Mode I, Q_I , at different normalised T-stress.

$T\sqrt{l_0}/K_{efj}$	-0.1	-0.075	-0.05	-0.025	0	0.025	0.05	0.075	0.1
Q_I	0.91	0.87	0.83	0.80	0.75	0.71	0.65	0.63	0.67

As previously, the LPA is employed to obtain the transition relative density constants, Q, in Eq. (11), given in Table 3 for several levels of T-stress. The remote boundary conditions were modified to account for the presence of T-stress, following Eqs. (4) and (5). The normalised values of T-stress are $-0.1 \le T \sqrt{l_0}/K_{eff} \le 0.1$, corresponding to $-1 \le B \le 1$ and $a = 40l_0$. For Mode I loading with negative T-stress, the onset of buckling can start at a larger relative density, e.g. for a lattice with fracture strain $\epsilon_0 = 0.01$ the transition relative density increases from 0.075 (T = 0) to 0.091 ($T \sqrt{l_0}/K_{eff} = -0.1$). For positive biaxiality regimes, the transition relative density is not significantly affected by the presence of the T-stress term.

The modified BLM is used to analyse the effects of the presence of T-stress on fracture toughness under Mode I loading. The deformation of the lattice in the vicinity of the pre-crack is shown in Fig. 10 for $T\sqrt{l_0}/K_{eff}=\{-0.1,0,0.1\}$, below the transition relative density ($\overline{\rho}=0.04$). 'F' shows the location of fracture and 'B' the first buckling strut. At T=0 and $T\sqrt{l_0}/K_{eff}=0.1$, fracture occurs ahead of the crack-tip in all examined relative densities; conversely, at $T\sqrt{l_0}/K_{eff}=-0.1$, fracture occurs at the first buckling strut.

The magnitude of T-stress affects the lattice deformation in two additional ways. First, the extent of the bending layers: for $T\sqrt{l_0}/K_{eff}=-0.1$, T=0 and $T\sqrt{l_0}/K_{eff}=0.1$, the compliant layer of buckled cells extends more than 150, 20 and 75 characteristic cell lengths (l_0) , respectively, from the crack-tip at the instant of fracture. Second, the direction of propagation of the compliant layer: negative T-stress shows buckling in the perpendicular direction, similar to T=0, and positive T-stress leads to buckling propagating backwards from the crack-tip at a 30-degree angle. Alongside the biaxial crack-tip fields, an increased likelihood of strut buckling with negative (compressive) T-stress is expected. In like manner, positive T-stress can promote tension induced buckling (Mane et al., 2021), leading to the reported extensive range of buckled struts.

The fracture toughness relative to the $T\sqrt{l_0}/K_{eff}=0$ case, $K_{\rm c}/K_{\rm c}$, $E_{\rm c}$, is shown in Fig. 11 for relative densities below and above the critical value, and T-stress range $-0.1 \le T\sqrt{l_0}/K_{eff} \le 0.1$. The fracture toughness of lattices that do not exhibit strut buckling is not significantly influenced by the presence of T-stress. However, T-stress

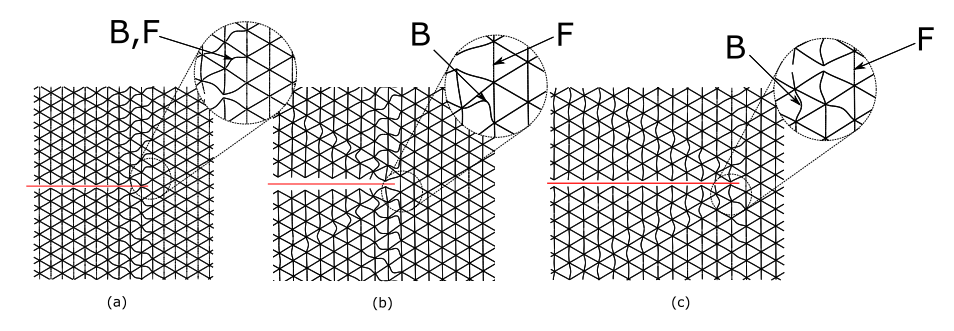


Fig. 10. Deformation mesh in a lattice with $\bar{\rho} = 0.04$ (below the transition relative density), at $T\sqrt{l_0}/K_{eff} = -0.1$ (a), T = 0 (b) and $T\sqrt{l_0}/K_{eff} = 0.1$ (c) under Mode I loading. Solid red lines indicate the pre-crack. Figures truncated to the vicinity of the crack-tip for the purpose of comparison.

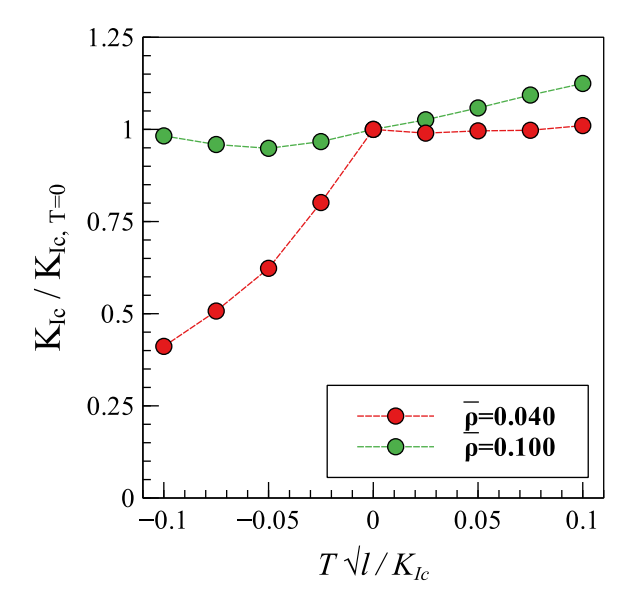


Fig. 11. Influence of T-stress on fracture toughness, relative to the fracture toughness in the absence of T-stress (B=0), below (red) and above (green) the buckling transition relative density.

can have a significant effect on the fracture of lattices after the onset of strut buckling: $K_{\rm Ic}$ decreases up to 41% relative to the T=0 case for negative T-stress, but remains unaffected for positive T-stress. The cases with significant knockdown in fracture toughness correspond to the range where the T-stress leads to fracture at the buckled strut.

To examine the effects of T-stress on the post-buckling fracture toughness scaling with $\overline{\rho}$, the procedure from Section 3.2 is repeated for lattices with $T\sqrt{l_0}/K_{eff}=-0.1$ and $T\sqrt{l_0}/K_{eff}=-0.05$ in Mode I. The scaling is shown in Fig. 12. Above the transition relative density the effects of T-stress are minimal; however, below the buckling transition relative density a new scaling regime is visible in which the knockdown is more severe the lower the relative density. The post-buckling scaling follows a power-law scaling with $d\approx 1.85$.

In summary, T-stress has a threefold effect: it increases the transition relative density, affects the orientation and length of the compliant layer of buckled cells, and leads to a knockdown in fracture toughness that is far more significant than the toughening shown in Fig. 5, transitioning to a scaling law with exponent d=1.85. It is concluded that the presence of T-stress should not be neglected in the testing and fracture toughness evaluation of such lattices, since idealised conditions where only the first term from the Williams expansion is relevant are not always achievable; for example, in Gu et al. (2019b) T-stress was present for fracture test-specimens of considerably large sizes. As such, the perceived toughening in Mode I may not always be replicable in finite-sized lattices.

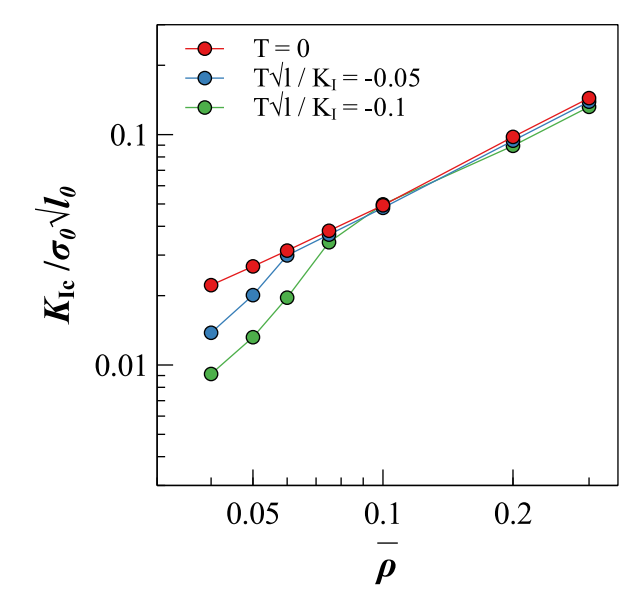


Fig. 12. Influence of *T*-stress on the scaling of fracture toughness with relative density in Mode I at different biaxiality ratios.

5. Conclusions

This study explored the influence of buckling struts on the fracture toughness of elastic-brittle triangular lattices. The results show that strut buckling prior to fracture may occur in physically relevant relative densities, e.g. for an indicative material with a fracture strain $\varepsilon_0=0.01$, the transition relative densities in Mode I and II are 0.075 and 0.212 respectively. When strut buckling precedes fracture, the scaling laws diverge from the currently established ones, showing a slight toughening in Mode I and a significant knockdown in Mode II. Fracture is activated prematurely in the buckled struts in Mode II.

The onset of buckling leads to the development of compliant layers of cells in the crack-tip vicinity which, in turn, influence fracture toughness. In Mode I, the compliant layers of cells result in crack-tip blunting, and act as a toughening mechanism. Furthermore, the compliant cells introduce variations in the local stiffness of the lattice. The most notable effect was observed in Mode II, where a local stiffness reduction of as much as 80% is developed in the vicinity of the crack-tip, and in the direction of the predicted fracture propagation.

In mixed-mode loading, the envelope of transition relative densities was bound by those of Modes I and II. Three regimes of influence of strut-buckling on the fracture toughness of a triangular lattices were identified: toughening in mode mixities with predominantly Mode I influence, no effect in mode mixities with approximately 25% Mode II influence, and knockdown in fracture toughness for modes with predominantly Mode II influence. The effect of higher-order stress

terms (*T*-stress) was also evaluated. Its influence was notable only after the onset of buckling in Mode I loading with negative *T*-stress contribution. There, it produces three effects: it increases the transition relative density, increases the size of the compliant layer of cells, and results in a knockdown in fracture toughness. Finally, the effect of buckling and higher-order terms on fracture toughness in finite-sized specimens warrants further investigation.

CRediT authorship contribution statement

Melle Gruppelaar: Writing – review & editing, Writing – original draft, Visualization, Validation, Methodology, Investigation, Formal analysis, Data curation, Conceptualization. Eral Bele: Writing – review & editing, Supervision, Project administration, Methodology. P.J. Tan: Writing – review & editing, Supervision, Resources, Project administration, Funding acquisition.

Declaration of competing interest

The authors declare that they have no known competing financial interests or personal relationships that could have appeared to influence the work reported in this paper.

Data availability

Data will be made available on request.

References

- Anderson, T.L., 1995. Fracture Mechanics: Fundamentals and Applications, second ed. CRC Press LCC, http://dx.doi.org/10.1201/9781315370293.
- Barenblatt, G.I., 1962. The mathematical theory of equilibrium cracks in brittle fracture. Adv. Appl. Mech. 7, 55–129. http://dx.doi.org/10.1016/S0065-2156(08)70121-2.
- Cherkaev, A., Ryvkin, M., 2019. Damage propagation in 2d beam lattices: 1. Uncertainty and assumptions. Arch. Appl. Mech. 89, 485–501. http://dx.doi.org/10.1007/ s00419-018-1429-z.
- Christodoulou, I., Tan, P.J., 2013. Crack initiation and fracture toughness of random Voronoi honeycombs. Eng. Fract. Mech. 104, 140–161. http://dx.doi.org/10.1016/ j.engfracmech.2013.03.017.
- Chuang, C.H., Huang, J.S., 2002. Effects of solid distribution on the elastic buckling of honeycombs. Int. J. Mech. Sci. 44, 1429–1443. http://dx.doi.org/10.1016/s0020-7403(02)00039-5.
- Cui, X., Xue, Z., Pei, Y., Fang, D., 2011. Preliminary study on ductile fracture of imperfect lattice materials. Int. J. Solids Struct. 48, 3453–3461. http://dx.doi.org/ 10.4028/www.scientific.net/KFM.535-536.18.
- Deng, B., Wang, S., Hartquist, C., Zhao, X., 2023. Nonlocal intrinsic fracture energy of polymerlike networks. Phys. Rev. Lett. 131, 228102. http://dx.doi.org/10.1103/ PhysRevLett.131.228102.
- Dugdale, D.S., 1960. Yielding of steel sheets containing slits. J. Mech. Phys. Solids 8, 100–104. http://dx.doi.org/10.1016/0022-5096(60)90013-2.
- Eischen, J.W., 1987. Fracture of nonhomogeneous materials. Int. J. Fract. 34, 3–22. http://dx.doi.org/10.1007/BF00042121.
- Erdogan, F., 1995. Fracture mechanics of functionally graded materials. Compos. Eng. 5, 753–770. http://dx.doi.org/10.1557/S0883769400048934.
- Fan, H., Jin, F., Fang, D., 2009. Uniaxial local buckling strength of periodic lattice composites. Mater. Des. 30, 4136–4145. http://dx.doi.org/10.1016/j.matdes.2009. 04.034.
- Fleck, N.A., Qiu, X.M., 2006. The damage tolerance of elastic-brittle, two-dimensional isotropic lattices. J. Mech. Phys. Solids 55, 562–588. http://dx.doi.org/10.1016/j. jmps.2006.08.004.
- Gibson, L.J., Ashby, M.F., 1997. Cellular Solids: Structure and Properties, second ed. Cambridge University Press, http://dx.doi.org/10.1017/CBO9781139878326.
- Gu, H., Li, S., Pavier, M., Attallah, M.M., Paraskevoulakos, C., Shterenlikht, A., 2019a. Fracture of three-dimensional lattices manufactured by selective laser melting. Int. J. Solids Struct. 180–181, 147–159. http://dx.doi.org/10.1016/j.ijsolstr.2019.07. 020.
- Gu, H., Pavier, M., Shterenlikht, A., 2018. Experimental study of modulus, strength and toughness of 2D triangular lattices. Int. J. Solids Struct. 152–153, 207–216. http://dx.doi.org/10.1016/j.ijsolstr.2018.06.028.
- Gu, H., Shterenlikht, A., Pavier, M., 2019b. Brittle fracture of three-dimensional lattice structure. Eng. Fract. Mech. 219, 106598. http://dx.doi.org/10.1016/j.engfracmech. 2019.106598.

- Guo, X.E., Gibson, L.J., 1999. Behavior of intact and damaged honeycombs: a finite element study. Int. J. Mech. Sci. 41, 85–105. http://dx.doi.org/10.1016/S0020-7403(98)00037-X.
- Haghpanah, B., Papadopoulos, J., Nayeb-Hashemi, H., Vaziri, A., 2014. Buckling of regular, chiral and hierarchical honeycombs under a general macroscopic stress state. Proc. R. Soc. A 170, 20130856. http://dx.doi.org/10.1098/rspa.2013.0856.
- He, Y., Zhou, Y., Liu, Z., Liew, K.M., 2018. Buckling and pattern transformation of modified periodic lattice structures. Extrem. Mech. Lett. 22, 112–120. http://dx.doi.org/10.1016/j.eml.2018.05.011.
- Hossain, M.Z., Hsueh, C.J., Bourdin, B., Bhattachary, K., 2014. Effective toughness of heterogeneous media. J. Mech. Phys. Solids 71, 15–32. http://dx.doi.org/10.1016/ j.jmps.2014.06.002.
- Hsieh, M.T., Deshpande, V.S., Valdevit, L., 2020. A versatile numerical approach for calculating the fracture toughness and R-curves of cellular materials. Int. J. Fract. 138, 103925. http://dx.doi.org/10.48550/arXiv.2003.01923.
- Huang, J.S., Gibson, L.J., 1991. Fracture toughness of brittle honeycombs. Acta Met. Mater. 7, 1617–1626. http://dx.doi.org/10.1016/0956-7151(91)90249-Z.
- Irwin, G.R., 1957. Analysis of stresses and strains near the end of a crack traversing a plate. J. Appl. Mech. 24, 361–364. http://dx.doi.org/10.1115/1.4011547.
- Kanninen, M.F., Popelar, C.H., 1985. Advanced Fracture Mechanics, first ed. OUP, http://dx.doi.org/10.1115/1.3269540.
- Kempen, K., Yasa, E., Thijs, L., Kruth, J.P., Van Humbeeck, J., 2011. Microstructure and mechanical properties of selective laser melted 18Ni-300 steel. Phys. Procedia 12, 255–263. http://dx.doi.org/10.1016/j.phpro.2011.03.033.
- Latture, R.M., Rodriguez, R.X., Holmes, L.R., Zok, F.W., 2018. Effects of nodal fillets and external boundaries on compressive response of an octet truss. Acta Mater. 149, 1429–1443. http://dx.doi.org/10.1016/j.actamat.2017.12.060.
- Leevers, P.S., Radon, J.C., 1982. Inherent stress biaxiality in various fracture specimen geometries. Int. J. Fract. 19, 311–325. http://dx.doi.org/10.1007/BF00012486.
- Li, Q., Chen, E.Y., Bice, D.R., Dunand, D.C., 2008. Mechanical properties of cast Ti-6Al-4V lattice block structures. Met. Mater. Trans. A 39, 441–449. http://dx.doi.org/10.1007/s11661-007-9440-y.
- Lipperman, F., Ryvkin, M., Fuchs, M.B., 2007. Fracture toughness of two-dimensional cellular material with periodic microstructure. Int. J. Fract. 146, 279–290. http://dx.doi.org/10.1007/s10704-007-9171-5.
- Luan, S., Chen, E., Gaitanaros, S., 2022. Energy-based fracture mechanics of brittle lattice materials. J. Mech. Phys. Solids 169, 105093. http://dx.doi.org/10.1016/j. imps.2022.105093.
- Mane, S., Khabaz, F., Bonnecaze, R.T., Liechti, K.M., Huang, R., 2021. A numerical study on elastic properties of low-density two-dimensional networks of crosslinked long fibers. Int. J. Solids Struct. 230–231, 111164. http://dx.doi.org/10.1016/j. iisolstr.2021.111164.
- Mane, S.M., Liechti, K.M., Huang, R., 2024. A numerical study on tensile strength of low-density kagome networks made of brittle fibers. Int. J. Solids Struct. 302, 112987. http://dx.doi.org/10.2139/ssrn.4734263.
- Noguchi, K., Fujita, M., Masaki, T., Mizushina, M., 1989. Tensile strength of yttriastabilized tetragonal zirconia polycristals. J. Am. Ceram. Soc. 72, 1305–1307. http://dx.doi.org/10.1111/j.1151-2916.1989.tb09736.x.
- Ohno, N., Okumura, D., Niikawa, T., 2004. Long-wave buckling of elastic square honeycombs subject to in-plane biaxial compression. Int. J. Mech. Sci. 46, 1697–1713. http://dx.doi.org/10.1016/j.ijmecsci.2004.09.011.
- Okumura, D., Ohno, N., Noguchi, H., 2004. Elastoplastic microscopic bifurcation and post-bifurcation behavior of periodic cellular solids. J. Mech. Phys. Solids 52, 641–666. http://dx.doi.org/10.1016/j.jmps.2003.07.002.
- Phani, A.S., Fleck, N.A., 2008. Elastic boundary layers in two-dimensional isotropic lattices. ASME J. Appl. Mech. 75, 0210201–0210208. http://dx.doi.org/10.1115/ 1.2775503
- Quintana-Alonso, I., Fleck, N.A., 2009. Compressive response of a sandwich plate containing a cracked diamond-celled lattice. J. Mech. Phys. Solids 57, 1545–1567. http://dx.doi.org/10.1016/j.jmps.2009.05.008.
- Quintana-Alonso, I., Mai, S.P., Fleck, N.A., Oakes, D.C.H., Twigg, M.V., 2010. The fracture toughness of a cordierite square lattice. Acta Mater. 58, 201–207. http: //dx.doi.org/10.1016/j.actamat.2009.08.069.
- Romijn, N.E.R., Fleck, N.A., 2007. The fracture toughness of planar lattices: Imperfection sensitivity. J. Mech. Phys. Solids 55, 2538–2564. http://dx.doi.org/10.1016/j.jmps.2007.04.010.
- Rousseau, C.E., Tippur, H.V., 2002. Evaluation of crack tip fields and stress intensity factors in functionally graded elastic materials: Cracks parallel to elastic gradient. Int. J. Fract. 114, 87–111. http://dx.doi.org/10.1023/A:1014889628080.
- Schmidt, I., Fleck, N.A., 2001. Ductile fracture of two dimensional cellular structures. Int. J. Fract. 111, 327–342. http://dx.doi.org/10.1023/A:1012248030212.
- Seiler, P.E., Tankasala, H.C., Fleck, N.A., 2019. The role of defects in dictating the strength of brittle honeycombs made by rapid prototyping. Acta Mater. 171, 190–200. http://dx.doi.org/10.48550/arXiv.1904.10362.
- Shanley, F.R., 1947. Inelastic column theory. J. Aeronaut. Sci. 14, 261–268. http://dx.doi.org/10.2514/8.1346.
- Sih, C.F., 1974. Small-scale yielding analysis of mixed mode plane-strain crack problems. In: STP560-EB Fracture Analysis: Proceedings of the 1973 Symposium on Fracture Mechanics, Part II. pp. 187–210. http://dx.doi.org/10.1520/STP33141S.

- Tankasala, H.C., Deshpande, V.S., Fleck, N.A., 2015. Crack-tip fields and toughness of two-dimensional elasto-plastic lattices. J. Appl. Mech. 82, http://dx.doi.org/10. 1115/1.4030666, 091004–10.
- Tankasala, H.C., Deshpande, V.S., Fleck, N.A., 2017. Tensile response of elastoplastic lattices at finite strain. J. Mech. Phys. Solids 109, 307–330. http://dx.doi.org/10. 17863/CAM.17636.
- Tankasala, H.C., Fleck, N.A., 2020. The crack-growth resistance of an elastoplastic lattice. Int. J. Solids Struct. 188–189, 233–243. http://dx.doi.org/10.1016/j.ijsolstr. 2019.10.007.
- Wang, A.J., McDowell, D.L., 2014. In-plane stiffness and yield strength of periodic metal honeycombs. J. Eng. Mater. Technol. 126, 137–156. http://dx.doi.org/10.1115/1. 1646165
- Werner, B., Červinek, O., Koutný, D., Reisinger, A., Pettermann, H.E., Todt, M., 2022.
 Numerical and experimental study on the collapse of a triangular cell under compression. Int. J. Solids Struct. 236–237, http://dx.doi.org/10.1016/j.ijsolstr. 2021.111295.
- Williams, M.L., 1957. On the stress distribution at the base of a stationary crack. J. Appl. Mech. 24, 109–114. http://dx.doi.org/10.1115/1.4011454.
- Xiao, L., Song, W., Wang, C., Liu, H., Tang, H., Wang, J., 2015. Mechanical behavior of open-cell rhombic dodecahedron Ti-6Al-4V lattice structure. Mater. Sci. Eng. A 640, 375–384. http://dx.doi.org/10.1016/j.msea.2015.06.018.
- Yang, M.Y., Huang, J.S., 2005. Elastic buckling of regular hexagonal honeycombs with plateau borders under uniaxial compression. Compos. Struct. 71, 229–237. http://dx.doi.org/10.1016/j.compstruct.2004.10.014.